Mutation of the Na+-K+-2Cl− cotransporter NKCC2 in mice is associated with severe polyuria and a urea-selective concentrating defect without hyperreninemia

Elisabeth Kemter,[1,2] Birgit Rathkolb,[1] Lise Bankir,[3] Anja Schrewe,[4,5] Wolfgang Hans,[5] Christina Landbrecht,[1] Matthias Klaften,[5] Boris Ivandic,[4] Helmut Fuchs,[5] Valérie Gailus-Durner,[5] Martin Hrabé de Angelis,[5] Eckhard Wolf,[1] Ruediger Wanke,[2] and Bernhard Aigner[1]

[1]*Chair for Molecular Animal Breeding and Biotechnology, and Laboratory for Functional Genome Analysis (LAFUGA), Gene Center, and* [2]*Institute of Veterinary Pathology, Center for Clinical Veterinary Medicine, LMU Munich, Munich;* [3]*INSERM Unité 872, Centre de Recherche des Cordeliers, Paris, France;* [4]*Department of Medicine III, Division of Cardiology, University of Heidelberg, Heidelberg; and* [5]*Institute of Experimental Genetics, Helmholtz Zentrum München, Neuherberg, and Chair for Experimental Genetics, Technische Universität München, Munich, Germany*

Submitted 7 September 2009; accepted in final form 8 March 2010

Kemter E, Rathkolb B, Bankir L, Schrewe A, Hans W, Landbrecht C, Klaften M, Ivandic B, Fuchs H, Gailus-Durner V, Hrabé de Angelis M, Wolf E, Wanke R, Aigner B. Mutation of the Na+-K+-2Cl− cotransporter NKCC2 in mice is associated with severe polyuria and a urea-selective concentrating defect without hyperreninemia. *Am J Physiol Renal Physiol* 298: F1405–F1415, 2010. First published March 10, 2010; doi:10.1152/ajprenal.00522.2009.— The bumetanide-sensitive Na+-K+-2Cl− cotransporter NKCC2, located in the thick ascending limb of Henle's loop, plays a critical role in the kidney's ability to concentrate urine. In humans, loss-of-function mutations of the *solute carrier family 12 member 1 gene* (*SLC12A1*), coding for NKCC2, cause type I Bartter syndrome, which is characterized by prenatal onset of a severe polyuria, salt-wasting tubulopathy, and hyperreninemia. In this study, we describe a novel chemically induced, recessive mutant mouse line termed *Slc12a1*^{I299F} exhibiting late-onset manifestation of type I Bartter syndrome. Homozygous mutant mice are viable and exhibit severe polyuria, metabolic alkalosis, marked increase in plasma urea but close to normal creatininemia, hypermagnesemia, hyperprostaglandinuria, hypotension,, and osteopenia. Fractional excretion of urea is markedly decreased. In addition, calcium and magnesium excretions are more than doubled compared with wild-type mice, while uric acid excretion is twofold lower. In contrast to hyperreninemia present in human disease, plasma renin concentration in homozygotes is not increased. The polyuria observed in homozygotes may be due to the combination of two additive factors, a decrease in activity of mutant NKCC2 and an increase in medullary blood flow, due to prostaglandin-induced vasodilation, that impairs countercurrent exchange of urea in the medulla. In conclusion, this novel viable mouse line with a missense *Slc12a1* mutation exhibits most of the features of type I Bartter syndrome and may represent a new model for the study of this human disease.

N-ethyl-*N*-nitrosourea; renin; solute carrier family 12 member 1

HEREDITARY DISEASES, INCLUDING nephropathies, are mainly caused by point mutations leading to gene dysfunction. For mimicking the situation of a hereditary disease in humans and analyzing the various facets of gene function and dysfunction, mutant mouse lines harboring ethylnitrosourea (ENU)-induced point mutations represent most suitable models (14). In the phenotype-driven Munich ENU-mutagenesis approach (12), several mouse models for kidney diseases were generated by screening for elevated plasma urea level (1). In one of these mutant mouse lines, line UREHR3, the causative mutation was identified within the *solute carrier family 12 member 1* (*Slc12a1*) gene, coding for the bumetanide-sensitive Na+-K+-2Cl− ion transporter NKCC2.

NKCC2 is expressed in the kidney in the apical membrane of the cells of the thick ascending limb of Henle's loop (TALH) and of the macula densa (8). This transporter plays a central role in the renal ability to concentrate urine and thus in the maintenance of body salt and water homeostasis. It is responsible for one of the major salt transport pathways in the kidney, which energizes and maintains the countercurrent multiplication mechanism. Besides salt reabsorption, regulation of acid-base and divalent mineral cation metabolism, NKCC2 also influences renin release and the tubuloglomerular feedback (TGF) mechanism. NKCC2 is the main pharmacological target of loop diuretics like bumetanide or furosemide (44).

Mutations of the *SLC12A1* gene in humans (OMIM 601678) were identified to cause type I Bartter syndrome (antenatal Bartter's disease, hyperprostaglandin E syndrome) (39). This is a hereditary recessive disease characterized by prenatal onset, a severe salt-wasting state with low blood pressure, metabolic alkalosis with hypokalemia, hyperreninemia, polyuria, hyperprostaglandinuria, and often hypercalciuria, in some cases associated with nephrocalcinosis (8, 29). Chronic use of loop diuretics like furosemide in humans causes a clinical phenotype similar to type I Bartter syndrome (6, 31, 42).

In this study, we performed a detailed genetic and phenotypic analysis of the Munich UREHR3 mutant mouse line harboring a novel allelic variant of NKCC2. Our phenotypic analyses especially aimed (1) at defining the mechanism by which this mutant ion transporter influences plasma urea levels, an effect that was not primarily expected for a salt transporter, and (2) at comparing the phenotype of the homozygous mutant mice with that described in type I Bartter syndrome in humans to unravel common features and potential discrepancies between these hereditary nephropathies.

MATERIALS AND METHODS

Animals, linkage analysis, and detection of the causative mutation. We undertook a detailed study of mouse line UREHR3 because homozygous mutant mice exhibited an increase in plasma urea which

was heritable in an autosomal recessive manner. The mouse line was established within the Munich ENU mouse mutagenesis project, which was carried out on the inbred C3HeB/FeJ (C3H) genetic background. An increase in the plasma urea level (cut-off level: 70 mg/dl, respectively, 11.7 mmol/l) was used as screening parameter to establish nephropathic ENU-induced mutant mouse lines. Mouse husbandry, breeding, linkage analysis, and genome-wide mapping were described previously (1). All mice had free access to drinking water and a standard rodent diet (V1124; Ssniff, Soest, Germany) ad libitum. The diet used contains a standard concentration of salts, 0.24% vol/vol sodium and 1.02% vol/vol potassium. All animal experiments were carried out under the approval of the responsible animal welfare authority.

Additional fine mapping was performed using further SNP and microsatellite markers. Subsequently, the *Slc12a1* gene was selected for sequence analysis. Sequence examination included cDNA sequences of all *Slc12a1* transcript variants (NCBI GenBank accession no. NM_183354, MMU20973, MMU20974, MMU20975 and MMU61381) both of two phenotypic homozygous mutant mice and of two C3H wild-type controls. Genotyping of mice was performed by allele-specific PCR and confirmed by restriction fragment length polymorphism (RFLP) analysis. Primer sequences are available upon request.

In addition, all other genes located between 120.3 Mb (rs8281409) and 130.5 Mb (rs6286476) on chromosome 2 were analyzed by using bioinformatic tools (http://services.nbic.nl/cgi-bin/copub3/CoPub.pl) with respect to their potential impact on renal function and renal diseases, ion and water transport, prostaglandin metabolism, regulation of blood pressure, or renin-angiotensin-aldosterone system (RAAS). Subsequently, genomic sequences of arginine vasopressin (*Avp*) and oxytocin (*Oxt*) were analyzed in both of two phenotypic homozygous mutant mice and of two C3H wild-type controls.

Analyses of clinical chemical parameters, plasma Nt-pro-atrial natriuretic peptide (Nt-proANP), plasma aldosterone, plasma renin concentration, and blood pressure measurements. Analyses of blood parameters were carried out in a series of mice of each genotype and gender as described previously (1). Plasma osmolality was calculated according to the formula: calculated $P_{osm} = 1.89 \times [Na^+] + 1.38 \times [K^+] + 1.03 \times [urea] + 1.08 \times [glucose] + 7.45$ (3). Blood-gas values were determined in Li-heparin blood samples using an ABL5 blood-gas analyzer (Radiometer, Willich, Germany). Plasma Nt-proANP concentrations were quantified using a commercial Nt-proANP (1–98) enzyme-linked immunosorbent assay (Biomedica Medizinprodukte, Vienna, Austria) (33). Plasma aldosterone concentration was measured by radioimmunoassay (Immunotech, Marseille, France). Therefore, EDTA plasma was collected by retroorbital bleeding under ether anesthesia from male mice between 12.00 and 14.30, and from female mice between 15.00 and 17.30. Plasma renin concentration (PRC) was measured by radioimmunoassay (Gammacoat, DiaSorin, Saluggia, Italy) using a fivefold dilution of 2 μl plasma, as the generation of angiotensin 1 (ANG I) after addition of excess rat substrate (18). ANG I generation was determined for a 1-h incubation period at 37°C and expressed as an hourly average. In each assay, background ANG I formation was determined by incubating substrate without plasma for the same time and subtracted from the plasma containing samples. In addition, background ANG I levels were determined in a plasma aliquot kept frozen without the addition of substrate until assaying. Blood for RPC determination was first collected under ether anesthesia. To exclude an influence of anesthesia on PRC values, PRC determination was repeated with blood samples collected from conscious mice by puncturing the submandibular vessels with a 19-gauge needle as described (23).

Blood pressure and heart rate were measured in the German Mouse Clinic (GMC) (7) in conscious mice by a noninvasive computerized tail-cuff method using the MC4000 Blood Pressure Analysis Systems (Hatteras Instruments, Cary, NC) (11). Measurements were carried out on 4 consecutive days with performance of 12 measurement runs in each session.

Analyses of urine and kidney function. Body weight, amount of water consumption, and urine excretion were measured in a series of mice of each genotype and gender, individually housed in metabolic cages (Tecniplast, Hohenpeissenberg, Germany). Mice had free access to food and drinking water for 2 days, followed by deprivation of water for 12 h. Urine was collected during *day 2* (for the steady-state study) and for the next 12 h (for the dehydration test). Homozygous *Slc12a1*[I299F] mutants and control animals (heterozygous mutants, wild-types) were analyzed simultaneously in pairs. Homozygous mutant mice exhibiting pyelonephritis were excluded from the analysis. Blood samples for measurement of plasma parameters were taken from the same mice 1 wk before urine collection. Urine osmolality was determined by freezing point depression analysis using a microosmometer (Bachofer, Reutlingen, Germany). Daily urine volume and concentration of electrolytes and proteins were measured, daily excretions were calculated, and data were normalized to 25 g body wt. As PGE_2 is rapidly metabolized, urinary excretion of PGE_2 was assayed with the Prostaglandin E metabolite EIA (Cayman, Ann Arbor, MI) measuring a stable derivate of PGE_2. Therefore, urinary prostaglandins were derivatized to a stable metabolite before assay.

Creatinine clearance was calculated according to the formula: creatinine clearance $= [Crea]_{24-h\ urine} \times$ 24-h urine volume/$[Crea]_{plasma}$. Data were normalized to 25 g body wt. Fractional excretion of a solute $\times$ (FE_x) was calculated according to the formula: $FE_x = ([x]_{24-h\ urine} \times$ 24-h urine volume)/$([x]_{plasma} \times$ creatinine clearance) $\times$ 100.

Skeletal analysis. Peripheral quantitative computed tomography (pQCT) analyses were performed in the GMC as described previously (7, 17).

Morphological kidney analysis. Histological analyses of kidneys were performed as described previously (1). In short, animals were killed by ether inhalation and kidneys were fixed via either orthograde vascular perfusion with or immersion in 4% paraformaldehyde in PBS (pH 7.2). After fixation, the kidneys were cut perpendicular to the longitudinal axis into 1- to 2-mm-thick slices, which were routinely processed and embedded in paraffin or in plastic. Staining of histological kidney sections included hematoxylin and eosin (H&E), Giemsa, and Masson trichrome. Kossa staining was used for demonstration of calcifications. The indirect immunoperoxidase technique served to localize NKCC2 using a rabbit polyclonal antibody against rat NKCC2, affinity-purified (1:100; Alpha Diagnostic International, San Antonio, TX). Immunohistochemistry of sections was carried out simultaneously under identical conditions.

Northern blot and Western blot analyses. Isolation of total RNA and Northern blotting were performed as described previously (16). Therefore, whole kidneys were homogenized in TRIzol (Invitrogen, Karlsruhe, Germany) for isolation of total RNA. The following primers were used to generate specific PCR probes: NKCC2 (forward: 5′-ATC TCA GTA GCT GGG ATG GAG-3′; reverse: 5′-ACA TTC AGC TCG GCG ATG AG-3′; 755 nt); Akr1b3 (forward: 5′-ATC ATG GCC AGC CAT CTG GAA C-3′; reverse: 5′-TGT CAC CAC GAT GCC TTT GCT G-3′; 627 nt); uromodulin (forward: 5′-TTG GAG TAC AGG CTG GAG TG-3′; reverse: 5′-AGT GAA GGT AGA CAA GGT CG-3′; 712 nt); renin (forward: 5′-ACT CTT GTT GCT CTG GAG TCC-3′; reverse: 5′-AAC CAG TGT CCA CCA CTA CC-3′; 839 nt); and GAPDH (forward: 5′-GTG GCA AAG TGG AGA TTG TTG CC-3′; reverse: 5′-GAT GAT GAC CCG TTT GGC TCC-3′; 290 nt). As RNA loading control, the GAPDH probe was used.

For Western blot analyses of NKCC2, cyclooxygenase (COX)-1, and COX-2, whole kidneys were homogenized in extraction buffer (20 mM Tris, 2% Triton X-100, 20% 5× Laemmli buffer). For expression analysis of renin, COX-1, and COX-2, homogenates of renal cortex and renal medulla were used. Protein concentration was determined by BCA assay. Equal amounts of proteins were loaded per lane on 8, 10, or 12% SDS-polyacrylamide minigels. Urine samples were standardized for equal creatinine levels. Blotting and immunodetection were performed as described previously (19). Equal protein
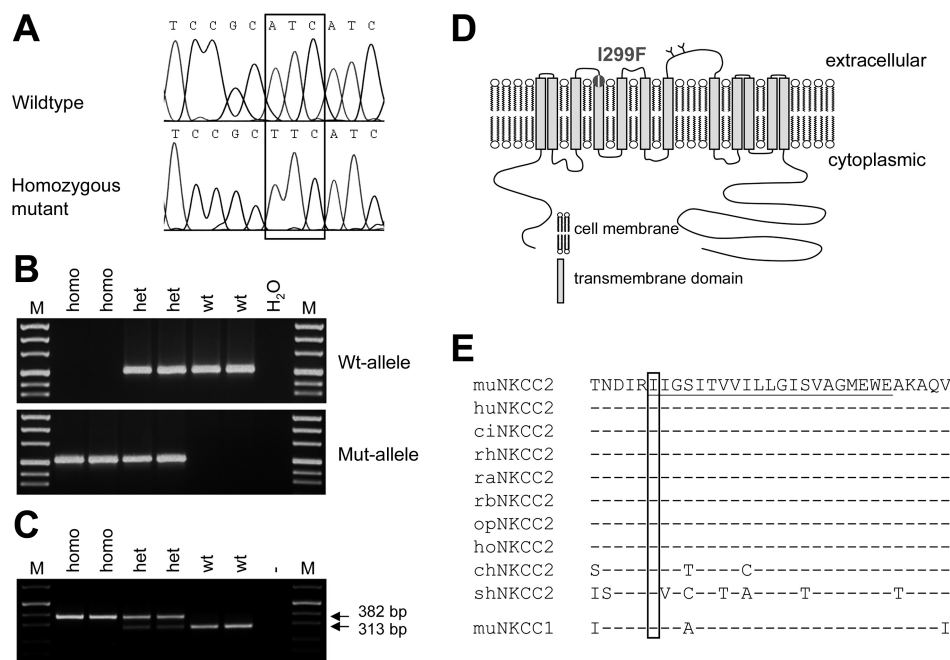
Fig. 1. Analysis of *Slc12a1* gene sequence in wild-type and mutant mice. *A*: electropherogram of the *Slc12a1* I299F mutation. The box shows the mutated codon, ATC (Ile) to TTC (Phe) at amino acid position 299. *B*: genotyping of mice by wild-type and mutant allele-specific PCR reaction, respectively. Homo, homozygous *Slc12a1*[I299F] mutant; het, heterozygous *Slc12a1*[I299F] mutant; wt, wild-type; M, pUC Mix 8 marker, MBI Fermentas. *C*: genotyping of mice by restriction fragment length polymorphism analysis. *Sfa*NI restriction digest of the 382-bp PCR product results in 313- and 69-bp (not included in figure) fragments in heterozygous mutant and wild-type animals. *D*: schematic topology of NKCC2 protein. The amino acid exchange from isoleucine to phenylalanine at position 299 of bumetanide-sensitive Na^+-K^+-$2Cl^-$ cotransporter (NKCC2) in *Slc12a1*[I299F] mutant mice is marked. *E*: amino acid conservation of mouse NKCC2 (residues 294–324). The region of the 4th transmembrane domain is underlined (residues 299–319). The boxed residue indicates isoleucine at position 299. Mu, mouse; hu, human; ci, chimpanzee; rh, rhesus monkey; ra, rat; rb, rabbit; op, opossum; ho, horse; ch, chicken; sh, shark.

loading was controlled by Ponceau staining. The following primary antibodies were used: rabbit polyclonal antibodies against rat NKCC2, affinity purified (1:1,000; Alpha Diagnostic International), rabbit polyclonal antibodies against murine COX-2, affinity purified (1:100; Cayman), rabbit polyclonal antibodies against murine COX-1, affinity purified (1:1,000; Cell Signaling, Frankfurt am Main, Germany), rabbit monoclonal antibodies against β-actin, affinity purified (1:1,000; Cell Signaling), chicken polyclonal antibodies against renin (1:500, generous gift of H. Castrop, Regensburg, Germany), rabbit monoclonal antibodies against GAPDH, affinity purified (1:1,000; Cell Signaling), and goat antiserum against human uromucoid (1:500; MP Biomedicals, Illkirch, France).

Statistical analysis. Data are shown as means ± SE. Data were analyzed by using paired or unpaired Student's *t*-tests or ANOVA as designated.

RESULTS

Establishment of Slc12a1[I299F] mutant mouse line. Generation of the chemically induced mutant mouse line UREHR3

Table 1. *Blood data in 3-mo-old mice*

	Male			Female		
	Wild-Type	Heterozygous	Homozygous	Wild-Type	Heterozygous	Homozygous
pH	7.34 ± 0.01	7.33 ± 0.01	7.43 ± 0.01‡	7.33 ± 0.01	7.31 ± 0.01	7.37 ± 0.01*
HCO_3^-, mmol/l	20.4 ± 0.5	21.7 ± 0.4	24.9 ± 0.5‡	18.7 ± 0.6	19.5 ± 0.3	21.4 ± 0.5†
Base excess, mmol/l	−3.9 ± 0.6	−3.2 ± 0.4	1.2 ± 0.4‡	−5.8 ± 0.7	−5.7 ± 0.5	−2.9 ± 0.5†
WBC, $10^3/\mu l$	6.0 ± 0.3	6.1 ± 0.3	6.5 ± 0.3	6.3 ± 0.3	5.6 ± 0.4	5.7 ± 0.3
RBC, $10^6/\mu l$	9.0 ± 0.1	8.7 ± 0.1	8.6 ± 0.1	9.0 ± 0.1	8.7 ± 0.3	9.2 ± 0.1
PLT, $10^3/\mu l$	730.0 ± 20.9	742.0 ± 16.2	656.0 ± 14.8‡	746.0 ± 24.5	751.0 ± 33.8	680.0 ± 25.3
Hemoglobin, g/dl	14.7 ± 0.2	14.5 ± 0.2	14.3 ± 0.1	14.7 ± 0.4	14.6 ± 0.5	15.2 ± 0.2
Hematocrit, %	45.9 ± 0.6	45.2 ± 0.7	44.2 ± 0.4	47.6 ± 0.6	46.2 ± 1.4	48.3 ± 0.4
Na, mmol/l	148.6 ± 0.3	148.6 ± 0.5	149.6 ± 0.5	47.6 ± 0.4	147.2 ± 0.6	147.4 ± 0.4
K, mmol/l	4.20 ± 0.08	4.14 ± 0.06	4.38 ± 0.08	4.04 ± 0.10	3.84 ± 0.07	4.08 ± 0.08
Ca, mmol/l	2.40 ± 0.00	2.40 ± 0.00	2.42 ± 0.02	2.38 ± 0.02	2.40 ± 0.00	2.58 ± 0.02‡
Cl, mmol/l	110.0 ± 0.3	109.1 ± 0.5	105.9 ± 0.6‡	110.7 ± 0.4	109.7 ± 0.4	106.3 ± 0.5‡
Mg, mmol/l	0.96 ± 0.01	1.04 ± 0.02†	1.27 ± 0.01‡	0.99 ± 0.03	0.98 ± 0.02	1.24 ± 0.03‡
P_i, mmol/l	1.82 ± 0.11	1.76 ± 0.07	1.92 ± 0.06	1.80 ± 0.12	1.72 ± 0.09	1.82 ± 0.10
Total protein, g/l	57.2 ± 1.3	55.6 ± 0.7	56.8 ± 0.9	56.8 ± 1.0	58.2 ± 1.1	59.2 ± 0.8
Creatinine, $\mu mol/l$	27.6 ± 0.6	27.4 ± 0.6	29.4 ± 0.6	30.0 ± 0.7	29.0 ± 0.3	33.3 ± 1.2*
Urea, mmol/l	9.3 ± 0.2	10.7 ± 0.3‡	21.2 ± 0.3‡	9.5 ± 0.3	10.4 ± 0.4	16.5 ± 0.8‡
Uric acid, $\mu mol/l$	98.6 ± 3.9	94.2 ± 3.1	100.9 ± 2.2	103.0 ± 5.7	98.3 ± 5.6	95.8 ± 6.2
Glucose, mmol/l	6.7 ± 0.5	5.4 ± 0.4	4.4 ± 0.3†	7.1 ± 0.4	6.8 ± 0.4	6.6 ± 0.4
Lactate, mmol/l	13.4 ± 0.2	14.2 ± 0.4	13.7 ± 0.3	11.1 ± 0.3	10.8 ± 0.3	11.1 ± 0.3
AP, U/l	107.6 ± 4.6	101.2 ± 4.1	119.0 ± 5.2	147.8 ± 3.5	153.8 ± 3.8	164.2 ± 5.8*
α-Amylase, U/l	2,374 ± 52	2,403 ± 56	2,585 ± 59*	1,938 ± 32	2,040 ± 44	2,413 ± 29‡
Lipase, U/l	55.3 ± 0.8	56.6 ± 1.2	68.1 ± 3.3†	59.4 ± 0.7	61.5 ± 1.1	76.7 ± 2.2‡
P_{osm} calc., mosmol/kgH_2O	310.9 ± 1.0	310.8 ± 1.1	322.8 ± 1.1‡	309.4 ± 0.7	309.0 ± 1.3	315.8 ± 1.0‡

Values are means ± SE; *n* = 10/genotype and gender. WBC, white blood cells; RBC, red blood cells; PLT, platelets; P_i, inorganic phosphorus; AP, alkaline phosphatase; P_{osm} calc., calculated plasma osmolality. Student's *t*-test vs. wild-type: *$P < 0.05$; †$P < 0.01$; ‡$P < 0.001$.

MOUSE MODEL OF BARTTER SYNDROME

and genome-wide linkage analysis to determine the chromosomal region of the causative mutation have been described previously (1). Increased plasma urea level was heritable in an autosomal recessive manner. Linkage analysis identified a single chromosomal site of the causative mutation on chromosome 2 between 120.3 (rs8281409) and 130.5 Mb (rs6286476), thereby excluding additional causative mutations outside the determined 10-Mb region. The probability of the existence of confounding nonsegregating mutations within this chromosomal region is $P < 0.001$ (15). Sequence analysis of $Slc12a1$ cDNA, whose gene is located at 124.8 Mb on chromosome 2, revealed an A→T transversion in exon 7 at nt 1127 (NCBI GenBank no. NM_183354) (Fig. 1A). Genotypic differentiation was enabled by allele-specific PCR reactions and was confirmed by RFLP analysis (Fig. 1, B and C). Mating of heterozygous mutant mice showed the expected Mendelian pattern of inheritance of the mutation in the offspring.

Additional bioinformatic analysis of the determined 10-Mb region (120.3–130.5 Mb) of chromosome 2 was carried out.

Within the 10-Mb region, 295 genes, markers, and QTLs are located; of them, 127 are Entrez Gene identifiers. Bioinformatic analysis of these genes revealed an impact of Avp and Oxt on ion transport, RAAS, and renin secretion. Subsequent sequencing detected no difference in the genomic sequence of Avp and Oxt between phenotypic homozygous mutant mice and C3H wild-type controls.

The identified mutation leads to an amino acid substitution from isoleucine to phenylalanine at position 299 of NKCC2, the protein derived from the $Slc12a1$ gene. Therefore, the line was designated as the $Slc12a1^{I299F}$ mutant mouse line. NKCC2 is a 12-transmembrane ion transporter and I299 is located at the first position of the fourth transmembrane-spanning domain (Fig. 1D). This region is well conserved among mammalian species (Fig. 1E). In addition, I299 is also conserved in NKCC1, another member of the $Slc12$ family exhibiting Na^+-K^+-$2Cl^-$ cotransporter activity.

Plasma composition and blood pressure in $Slc12a1^{I299F}$ mutant mice. In addition to an enhanced plasma urea concentration, 3-mo-old homozygotes of both genders exhibited hy-
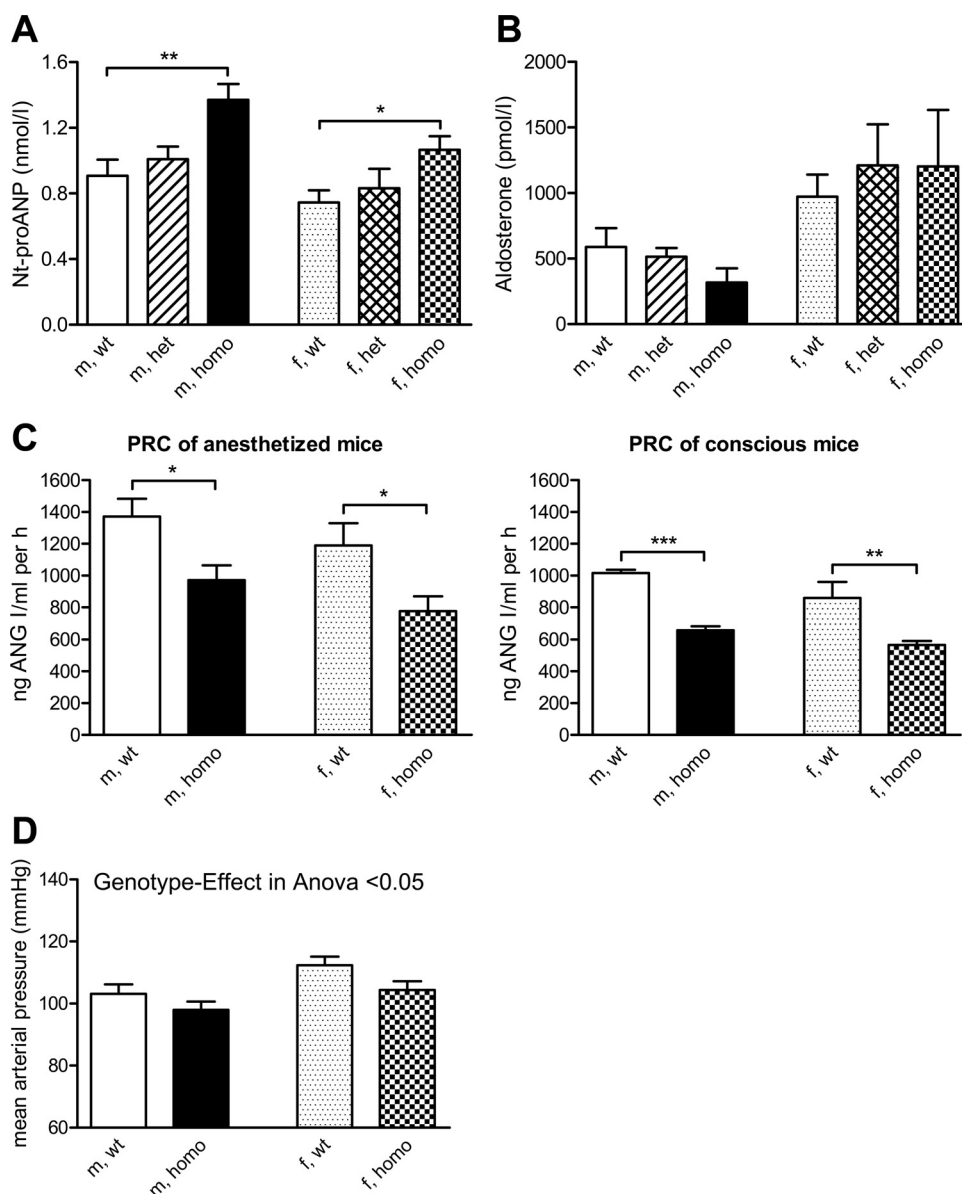

Fig. 2. Analyses of N-terminal propeptide of the atrial natriuretic peptide (Nt-proANP), plasma aldosterone concentration, plasma renin concentration (PRC), and mean arterial blood pressure in 3-mo-old mice. *A*: Nt-proANP is significantly increased in homozygous mutants; $n = 5$–8/genotype and gender. *B*: plasma aldosterone concentration is not significantly different between different genotypes; $n = 5$–9/genotype and gender. *C*: PRC of anesthetized and conscious mice is significantly lower in homozygous mutants than in sex-matched wild-type control mice; $n = 4$–7/genotype and gender. *D*: mean arterial blood pressure is significantly lower in homozygous mutants than in wild-type control mice; $n = 12$/genotype and gender. Wt, wild-type; het, heterozygous mutant; homo, homozygous mutant; n, number of animals analyzed. Bars represent means $\pm$ SE. Student's *t*-test vs. wild-type: *$P < 0.05$; **$P < 0.01$.

pochloremic metabolic alkalosis and hypermagnesemia (Table 1). Female homozygous mutants had hypercalcemia and an increase in alkaline phosphatase activity in plasma. Nt-proANP was significantly increased in homozygous mutants of both genders (Fig. 2A). No genotypic difference was detected in plasma aldosterone concentration (Fig. 2B).

A characteristic feature of NKCC2 dysfunction in humans is the occurrence of hyperreninemia. PRC in homozygous mutant mice was significantly lower than that in wild-type littermate controls in blood samples collected under anesthesia (Fig. 2C). This phenotypic difference was still apparent when blood was drawn from conscious mice, although values in both genotypes were lower than those obtained under anesthesia.

Mean arterial blood pressure (Fig. 2D) as well as systolic and diastolic pressures (not shown) were significantly decreased in homozygous mutants. Heart rate did not differ significantly between genotypes (not shown).

To obtain phenotypic data from earlier stages, analysis of blood chemistry was carried out 7-wk postpartum and detected already twofold higher plasma urea and modestly higher plasma creatinine as well as hypochloremia in homozygous mutants compared with their wild-type controls (not shown). To obtain data about the progression of the phenotype, blood parameters were also analyzed in 6-mo- and 1-yr-old mice, revealing that the phenotype did not change with age (not shown).

No striking pathological symptoms like obvious polyhydramnios were observed during pregnancy. The suckling period appeared normal among the three genotypes. Furthermore, we observed no obvious differences in behavior or fertility.

Body weight, urine excretion, and concentrating ability. Three-month-old homozygous mutants had a slightly lower body weight than heterozygotes and wild-type mice, but the difference was not significant (Table 2). A three- to fourfold increase in daily urine volume and a decrease in urine osmolality were detected in 3-mo-old homozygous mutant mice compared with heterozygous mutants and wild-type controls. Low urinary excretion of glucose excluded osmotic diuresis as the cause of polyuria. Interestingly, calculation of the urine-to-plasma concentration ratio (U/P) for total osmoles and for each individual solute showed that this urinary concentrating defect did not affect all solutes equally. The U/P ratios for urea and for uric acid were reduced in homozygotes compared with wild-type mice much more than those for all osmoles together or for creatinine, sodium, or potassium (not shown).

Daily urinary excretion of creatinine, urea, sodium, and potassium was significantly increased by 10–60% in homozygous mutants of both genders. Homozygotes also exhibited a fourfold increase in calcium and magnesium excretion and a twofold decline in uric acid excretion. Creatinine clearance was 10–30% higher in homozygous mutants than in heterozygotes or wild-type mice (significant only in males) (Fig. 3). FE of the different solutes was differently affected by the genotype. FE_{urea} was strongly decreased in homozygotes, while FE_{Na} and FE_K were fairly unchanged or slightly increased. This indicates a "urea-selective" handling defect in homozygous mutants. FE of uric acid was decreased to about the same extent as that of urea, but this was mainly due to a twofold reduction in its daily excretion. In contrast, FE_{Ca} and FE_{Mg} were markedly increased in both genders (more than 3-fold for Ca and 1.5-fold for Mg). Daily urinary excretion of PGE_2 was approximately doubled in male homozygous mutants and also significantly increased in female homozygotes compared with wild-type controls (Table 2). Uromodulin excretion was markedly reduced (see below).

To further test urine concentrating ability, animals were deprived of drinking water for 12 h (Table 3). Homozygous mutants lost >13% of body weight, about twofold more than heterozygotes or wild-type mice, and they only slightly increased urine osmolality, in contrast to wild-type mice.

Pathomorphological kidney findings. Morphological examinations were performed in 3- to 18-mo-old animals (145 mice in total, 62 of which were homozygotes). No obvious differences were detected between kidneys of heterozygous mutant and wild-type mice. In contrast, kidneys of homozygous mutants exhibited several abnormalities (Fig. 4). Uni- or bilateral dilation of the renal pelvis of varying severity associated with atrophy of the renal papilla was frequently found in homozy-

Table 2. *Body weight, water intake, and urinary data in 3-mo-old mice*

	Male			Female		
	Wild-Type	Heterozygous	Homozygous	Wild-Type	Heterozygous	Homozygous
Body weight, g	27.3 ± 0.5	27.9 ± 0.5	26.9 ± 0.6	25.6 ± 0.3	25.7 ± 0.6	24.0 ± 0.7
Water intake, ml/day	4.9 ± 0.4	4.9 ± 0.6	12.5 ± 1.1‡	10.4 ± 1.4	7.3 ± 0.9*	15.0 ± 1.5*
Urine volume, ml/day	1.5 ± 0.1	1.4 ± 0.2	6.9 ± 0.4‡	2.3 ± 0.4	1.9 ± 0.2	7.6 ± 0.5‡
Urine osmolality, mosmol/kgH$_2$O	3,177 ± 134	3,354 ± 378	814 ± 25‡	2,871 ± 272	2,944 ± 218	889 ± 34‡
Na, μmol/day	280.1 ± 21.8	284.1 ± 26.1	372.8 ± 19.8*	357.5 ± 34.6	310.2 ± 20.1	411.3 ± 25.3
K, μmol/day	591 ± 47	581 ± 65	946 ± 72†	726 ± 86	621 ± 38	1,100 ± 66‡
Ca, μmol/day	2.7 ± 0.2	2.7 ± 0.3	12.5 ± 0.8‡	4.1 ± 0.5	3.4 ± 0.6	16.5 ± 1.4‡
Cl, μmol/day	459.9 ± 34.6	467.6 ± 42.5	524.9 ± 42.6	583.9 ± 52.5	528.7 ± 23.3	649.7 ± 35.8
Mg, μmol/day	18.5 ± 1.6	18.4 ± 2.2	51.4 ± 3.2‡	28.7 ± 4.4	24.2 ± 2.3	67.9 ± 7.2‡
P$_i$, μmol/day	278.3 ± 19.4	271.7 ± 24.3	388.9 ± 44.7	ND	ND	ND
Creatinine, μmol/day	5.63 ± 0.40	5.66 ± 0.52	8.08 ± 0.26†	7.94 ± 0.52	7.54 ± 0.34	9.25 ± 0.37†
Urea, mmol/day	2.77 ± 0.22	2.75 ± 0.25	3.59 ± 0.19*	3.51 ± 0.24	3.27 ± 0.16	3.94 ± 0.26†
Uric acid, μmol/day	0.54 ± 0.04	0.53 ± 0.06	0.23 ± 0.02‡	1.26 ± 0.14	1.09 ± 0.14	0.69 ± 0.07†
Glucose, μmol/day	2.87 ± 0.21	2.63 ± 0.21	2.20 ± 0.52	7.06 ± 1.06	4.14 ± 0.37†	3.27 ± 0.72†
Total protein, mg/day	11.1 ± 1.0	11.1 ± 1.3	22.7 ± 1.4‡	7.6 ± 0.8	9.0 ± 0.7	6.2 ± 0.7
Albumin, μg/day	21.3 ± 2.6	19.0 ± 1.4	12.7 ± 2.4‡	22.4 ± 3.4	17.0 ± 0.9	9.3 ± 0.7†
PGE$_2$-M, ng/day	2.3 ± 0.2	2.5 ± 0.3	4.4 ± 0.3‡	15.3 ± 1.4	13.2 ± 1.0	20.3 ± 1.2*

Values are means ± SE, standardized on 25-g body weight; $n = 8$/genotype and gender. PGE$_2$-M, prostaglandin E$_2$ metabolite; ND, not determined. Student's *t*-test vs. wild-type: *$P < 0.05$; †$P < 0.01$; ‡$P < 0.001$.
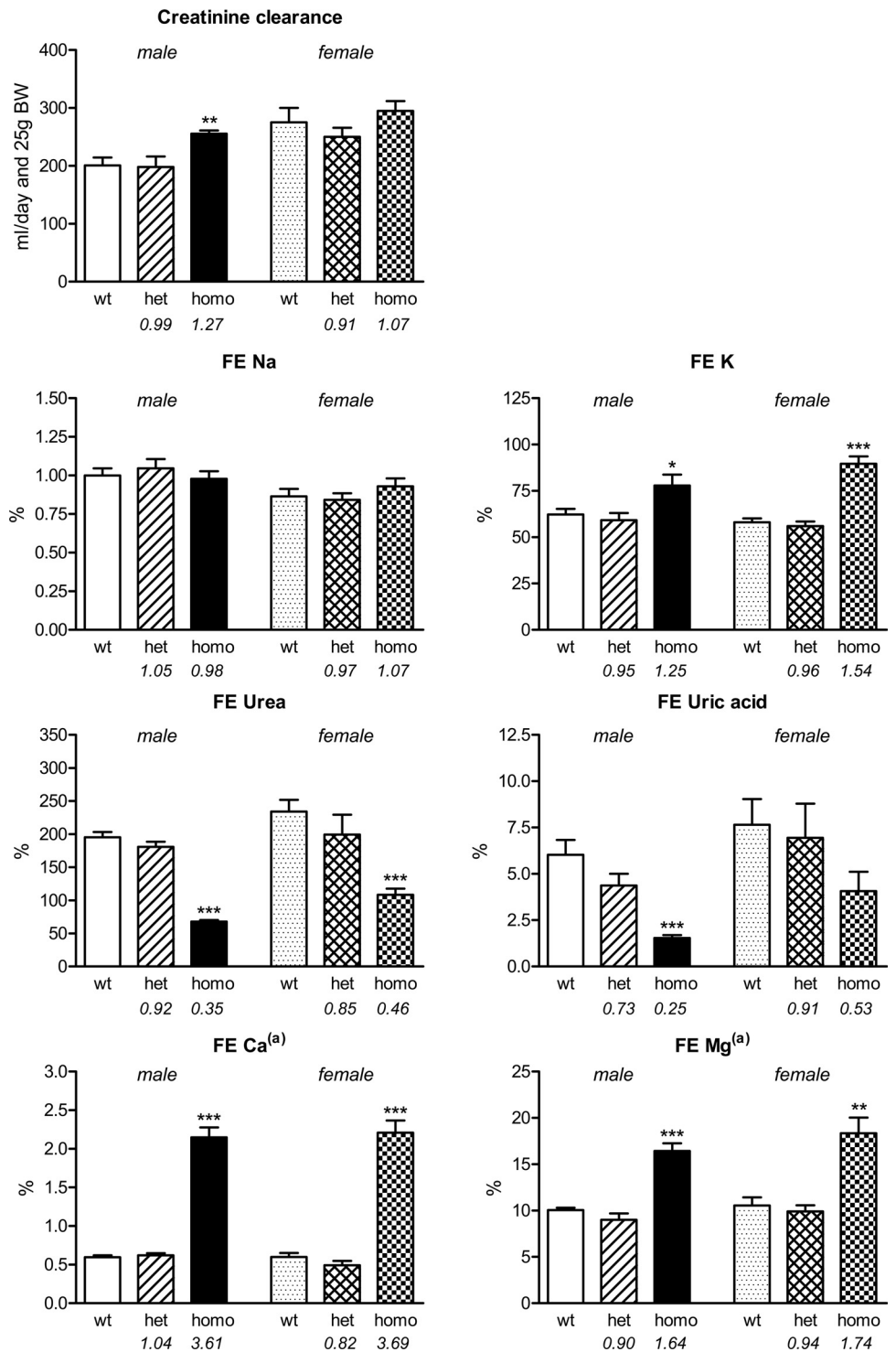
Creatinine clearance

Fig. 3. Creatinine clearance and fractional excretion (FE) of Na, K, urea, uric acid, Ca, and Mg in 3-mo-old mice. (a): Plasma values used for the calculation of Ca and Mg fractional excretions are the means shown in Table 1, because Ca and Mg concentrations were not measured in the plasma of these mice. It is expected that this does not lead to any bias, because there are little interindividual variations in plasma Ca and Mg and because both series of mice were in steady state with the same dietary conditions. Thus their plasma values were estimated to be similar. Values are means ± SE. Creatinine clearance was standardized on 25-g body weight. Ratios relative to wild-type values are indicated in italics; $n = 7$–8/genotype and gender. Student's t-test vs. wild-type: $*P < 0.05$; $**P < 0.01$; $***P < 0.001$.

gotes (Fig. 4A). This lesion appeared to be more pronounced in males and worsened with age. Furthermore, focal calcification of interstitium and tubular epithelial cells was occasionally detected in these mice (Fig. 4B). Male homozygotes often had variable degrees of chronic purulent pyelitis (Fig. 4, C and D). Few homozygous mutant males (4 of 45) exhibited a purulent pyelonephritis progressing to end-stage kidneys (not shown). Bacteriological analysis of spot urine of homozygous mutant males detected *Enterobacteriaceae* as unspecific germ flora.

Expression analyses of NKCC2, aldose reductase (Akr1b3), renin, COX-1 and -2, and uromodulin in the kidney. In whole kidney tissue samples, no alterations in NKCC2 mRNA transcript abundance were detected between genotypes (Fig. 5A). In contrast, NKCC2 protein abundance was strongly reduced in homozygous mutant mice compared with heterozygous mutant and wild-type mice (Fig. 5B). In kidney sections, mutant NKCC2 was located at the apical membrane of TALH cells; however, the signal was less intense than in wild-type controls

Table 3. *Urinary concentrating ability in 3-mo-old mice after deprivation of drinking water for 12 h*

	Male			Female		
	Wild-Type	Heterozygous	Homozygous	Wild-Type	Heterozygous	Homozygous
Urine volume, ml	0.6 ± 0.1	0.6 ± 0.1	$1.8 \pm 0.2\ddagger$	0.4 ± 0.1	0.4 ± 0.0	$1.4 \pm 0.2\dagger$
Urine osmolality, mosmol/kgH$_2$O	$4,126 \pm 302$	$3,516 \pm 210$	$1,029 \pm 27\ddagger$	$4,672 \pm 323$	$4,439 \pm 230$	$1,388 \pm 103\ddagger$
Loss of body weight, %	6.1 ± 0.5	5.6 ± 0.6	$13.5 \pm 0.8\ddagger$	6.6 ± 0.3	$7.9 \pm 0.3*$	$13.8 \pm 0.8\ddagger$

Data are means $\pm$ SE; $n = 8$ per genotype and gender. Student's *t*-test vs. wild-type: $*P < 0.05$; $\dagger P < 0.01$; $\ddagger P < 0.001$.

(Fig. 4, *E* and *F*). Akr1b3 transcript abundance was strongly reduced in homozygous mutant mice compared with heterozygotes and wild-type mice (Fig. 5*A*). Renin mRNA transcript abundance was slightly decreased in homozygotes compared with sex-matched heterozygotes and wild-type animals (Fig. 5*A*). No genotype difference in renin protein abundance in the renal cortex was detected (Fig. 5*C*). No obvious difference in COX-1 and COX-2 protein expression in whole kidney lysates (Fig. 5*B*) as well as in renal cortex and renal medulla (Supplementary Fig. S1; all supplementary material for this article is available on the journal web site) was detected between the
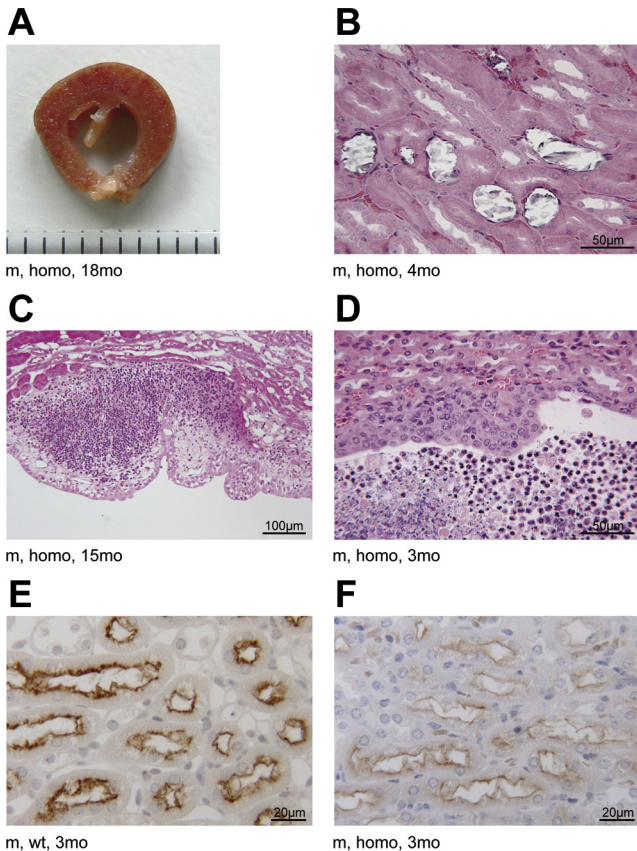

Fig. 4. Pathological and immunohistochemical findings in kidneys of homozygous mutant mice. *A*: kidney lamella of an 18-mo-old male homozygous mutant exhibiting moderate hydronephrosis (scale bar in mm). *B*: kidney section of a 4-mo-old male homozygous mutant exhibiting focal calcifications [hematoxylin and eosin (H&E), plastic section]. *C*: kidney section of a 15-mo-old male homozygous mutant exhibiting purulent pyelitis (H&E, plastic section). *D*: kidney section of a 3-mo-old male homozygous mutant exhibiting purulent pyelitis with purulent exudate and bacteria in the renal pelvis (H&E, paraffin section). *E* and *F*: immunohistochemical localization of NKCC2 on the apical membrane of thick ascending limb of the loop of Henle (TALH) cells in a 3-mo-old male wild-type mouse (*E*) and a male homozygous mutant (*F*). The signal intensity in the homozygous mutant is less intense.

different genotypes. Uromodulin mRNA transcript abundance was slightly decreased in homozygous mutant mice of both genders (Fig. 5*A*). Urinary excretion of uromodulin was markedly decreased in homozygotes, whereas it was moderately decreased in heterozygotes (Fig. 5*D*).

Skeletal analysis. To elucidate the long-term effect of hypercalciuria, skeletal analysis was performed. Femoral cortical bone mineral density was significantly reduced in 9-mo-old homozygous mutants compared with wild-type mice, indicating osteopenia (Fig. 6). Additionally, total bone content and total bone area were significantly decreased in male homozygous mutants by 8–15% ($P < 0.001$; not shown).

DISCUSSION

Homozygous *Slc12a1*[I299F] mutant mice exhibit a single amino acid substitution in NKCC2. They are viable and grow and reproduce normally. This study confirms their markedly increased plasma urea concentration but shows that this is not due to renal failure. Their plasma creatinine is only slightly elevated, and their creatinine clearance is higher than in wild-type mice. Homozygous mutants show a severe defect in their ability to concentrate urine, leading to increased urine output and water consumption. In addition, their calcium and magnesium excretion is markedly increased and their uric acid excretion is reduced.

In contrast to this new mouse line, mice with a complete lack of the NKCC2 cotransporter obtained by targeted disruption of the *Slc12a1* gene, although born normally, died within the first 2 wk postpartum, due to severe renal failure and metabolic alterations. Treatment with the COX inhibitor indomethacin from *day 1* onward for 3 wk rescued only 10% of the homozygous knockout mice (43). Isoform-specific knockouts generated by targeted disruption of isoform-specific exon 5 of the *Slc12a1* gene exhibited minor phenotypic alterations. Mice deficient in either NKCC2 isoform A or B showed an altered TGF function curve (22, 23).

NKCC2 in the TALH is strongly involved in the build-up and maintenance of salt accumulation in the medulla, a main step in the urine concentrating mechanism (8). The polyuria of homozygous *Slc12a1*[I299F] mutants may be due to a reduction in NaCl transport in the TALH resulting from a lesser ion transport capacity of the mutant protein and from a reduced expression of this protein in the TALH. The mutation might alter the transport capacity of NKCC2 because it is located in the fourth transmembrane-spanning domain which is involved in ion binding (13). All NKCC2 isoforms might be equally affected by the NKCC2 dysfunction, as the I299F exchange is not located in an isoform-specific region. The assumption that NaCl transport is reduced in the TALH of mutant mice is strongly supported by the marked increase in Mg^{2+} and Ca^{2+} excretion because the reabsorption of these ions in the TALH

A

heterozygous | homozygous | wildtype

NKCC2

Akr1b3

Renin

Umod

GAPDH

B

heterozygous | homozygous | wildtype

NKCC2

COX-2

COX-1

β-actin

C

homozygous | wildtype
0.99 ± 0.25 | *1.00 ± 0.16*

Renin

GAPDH

D

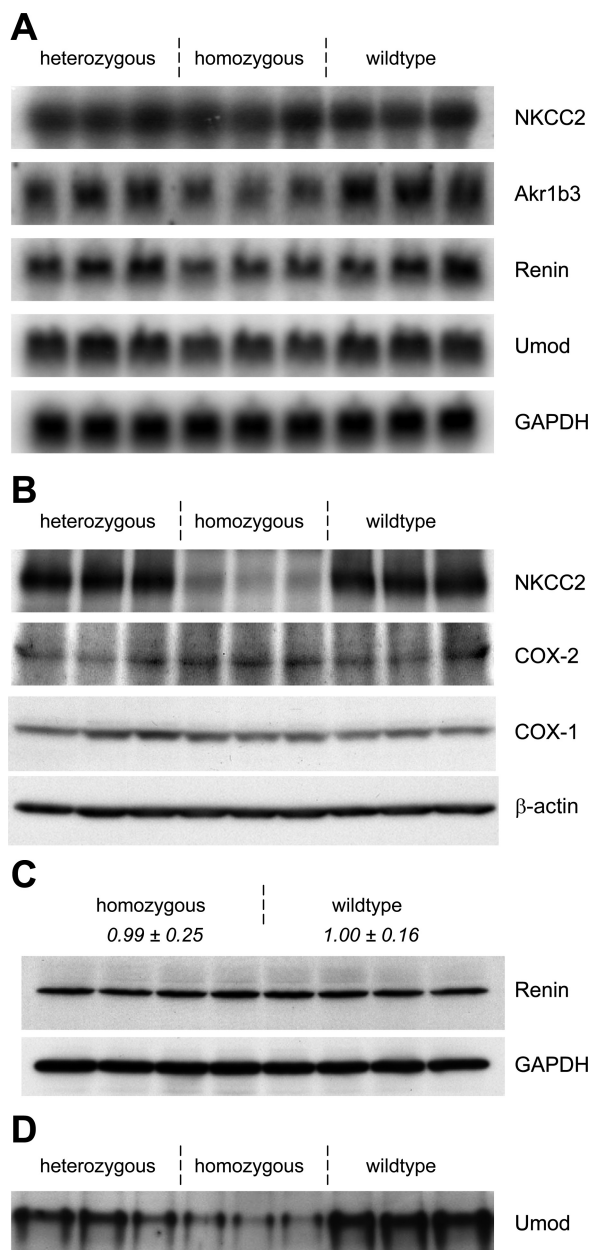heterozygous | homozygous | wildtype

Umod

Fig. 5. Expression analyses of NKCC2, Akr1b3, renin, cyclooxygenase (COX)-1, COX-2, and uromodulin (Umod) in the kidney. *A*: Northern blot analysis of mRNA abundance of NKCC2, Akr1b3, renin, and uromodulin in kidneys of 3-mo-old mice. *B–D*: Western blot analysis of NKCC2, COX-1, and COX-2 in whole kidney lysates (*B*), renin in lysates of renal cortex (*C*), and uromodulin in urine (*C*) of 3-mo-old mice. *C*: equal loading of COX-1 immunoblot was controlled by immunoblotting with β-actin antibody. Signal intensities of renin protein expression in renal cortex were quantified and correlated to GAPDH expression. Italic numbers indicate means ± SD of renin expression by defining the mean of the wild-type renin signal as 1.0.

is known to be driven by the transepithelial potential difference generated by NKCC2 transport activity (8, 9). Impaired NKCC2 ion transport activity, caused by a putatively altered ion transport capacity due to the mutation and/or reduced protein abundance of mutant NKCC2, might result in a defect in medullary solute accumulation as suggested by the reduced abundance of aldose reductase Akr1b3, an enzyme known to be well correlated with local medullary hypertonicity produced

by the activity of NKCC2 (20). However, NKCC2 activity is not completely abolished in mutant mice because they are able to concentrate urine up to about two to three times plasma osmolality (vs. 10–12 times in wild-type mice). The extent of ion transport deficiency of mutant NKCC2 needs to be evaluated in isolated, perfused TALH or in transfected *Xenopus laevis* oocytes.

How can an impairment in NKCC2-mediated transport in the TALH result in a selective defect in urine urea concentration and a doubling of the plasma urea level? The TALH is not known to transport urea, and its function is not likely to affect that of urea transporters located in different structures. Urea concentration in the urine depends on the sequestration of concentrated urea in the inner medulla. This is achieved by the sustained delivery of urea in the inner medullary interstitium by the terminal collecting ducts through the vasopressin-dependent urea transporter UT-A1, and by complex intrarenal urea recycling that prevents urea escape from the kidney and maintains a high osmotic pressure in the inner medulla. This recycling involves an intense countercurrent exchange of urea between venous (ascending) and arterial (descending) vasa recta that run in parallel and opposite directions in the inner medulla and within the vascular bundles of the outer medulla (45). A relatively low medullary blood flow is critical for efficient urea recycling by offering a sufficient contact time for urea exchange between ascending and descending vasa recta blood. The rise in urinary PGE_2 excretion in mutant mice suggests an increased production of renal medullary PGE_2. PGE_2 is known to increase medullary blood flow (5, 41). Thus it is possible to assume that the capacity of mutant mice to concentrate urea in the urine was more severely impaired than the overall capacity to concentrate urine because an increased medullary blood flow due to enhanced vasodilatory PGE_2 impaired intrarenal urea recycling. As a result, more of the urea delivered to the inner medulla by the terminal collecting ducts returned to the general circulation by the ascending vasa recta merging with renal veins at the corticomedullary border and thus contributed to the rise in plasma urea. This hypothesis needs to be validated by studying the influence of prostaglandin inhibition on urine concentrating ability and U/P ratio for urea in mutant mice. Interestingly, inhibition of prostaglandin synthesis by COX inhibitors considerably ameliorates the urinary concentrating ability and reduces fluid loss in patients with type I Bartter syndrome (28, 29). In the homozygous *Slc12a1*[I299F] mutant mice, the site and cause of increased PGE_2 synthesis have to be elucidated. Although no alterations in renal COX-1 and COX-2 protein abundances were detected, increased enzymatic activity of COX-1 or COX-2 in homozygous mutant mice could be the source of increased urinary PGE_2 excretion.

Besides the effect on the urine concentrating mechanism, mutant NKCC2 caused a broad spectrum of phenotypic alterations in homozygous *Slc12a1*[I299F] mutant mice. Similar to type I Bartter syndrome in humans, homozygous mutant mice exhibited distinct metabolic alterations including azotemia, metabolic alkalosis, polyuria, hypercalciuria, kaliuresis, hyperprostaglandinuria, low blood pressure, and increased blood ANP levels. In mutant mice, impaired NKCC2-mediated ion transport resulted in hypercalciuria and hypermagnesiuria, associated with mild nephrocalcinosis. The osteopenic phenotype as well as increased plasma calcium and alkaline phosphatase
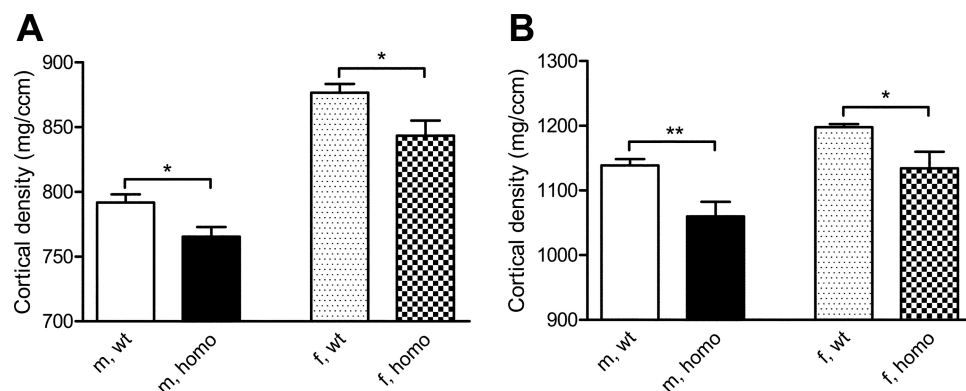
Fig. 6. Skeletal analysis of cortical bone mineral density (BMD) by peripheral quantitative computed tomography (pQCT). BMD was determined in 9-mo-old wild-type and homozygous $Slc12a1^{I1299F}$ mutant mice. *A*: distal femoral metaphysis. *B*: femoral diaphysis. BMD of homozygous mutant mice were significantly lower than in wild-type control mice, demonstrating an osteopenic phenotype in homozygous mutant mice; $n = 8–10$/genotype and gender. Bars represent means ± SE. Student's *t*-test vs. wild-type: $*P < 0.05$; $**P < 0.01$.

activity suggest a higher bone turnover and/or a defect in bone mineralization in homozygotes. In humans suffering from antenatal Bartter syndrome, occurrence of nephrocalcinosis due to hypercalciuria and osteopenia was often described (28, 37), and loss of bone mass was assumed to be a consequence of hypercalciuria (30).

Homozygous mutant mice had a significantly decreased daily excretion and reduced FE of uric acid. Decreased uric acid clearance was also described in humans with type I Bartter syndrome (27). Tubular reabsorption of urate is located in the proximal tubule and mediated by urate transporters (4). NKCC2 does not primarily affect tubular urate reabsorption. However, mutant NKCC2 and the resulting polyuria might affect urate transport indirectly, by inducing secondarily an increase in proximal sodium reabsorption. This is known to promote the proximal reabsorption of urate (38) and has been described in the heritable human "uromodulin-associated kidney disease" (35). The absence of hyperuricemia in homozygous mutant mice might be due to the uricase activity present in rodents but absent in humans (4).

Homozygotes excreted considerably less uromodulin than wild-type mice and heterozygous mutants. In humans suffering from antenatal Bartter syndrome, a marked reduction of uromodulin synthesis and urinary excretion has also been described (34). One function of uromodulin, the most abundant urinary protein in mammals, might be to protect the kidney from ascending urinary tract infections (2, 21, 25). Some male homozygous mutant mice showed mild purulent pyelitis and purulent pyelonephritis. Recurrent urinary tract infections were reported in some patients suffering from type I Bartter syndrome (26).

Besides these similarities, a few features observed in homozygous mutant mice differ from those described in patients with type I Bartter syndrome. The results concerning the hormonal systems that influence sodium handling by the kidney (renin and aldosterone) diverge from what is currently reported for the human syndrome. Hyperreninemia is observed in the human syndrome or during chronic NKCC2 inhibition by furosemide (6, 8, 36). In contrast, homozygous $Slc12a1^{I1299F}$ mutant mice exhibited a moderate decrease in PRC and renal renin mRNA transcript abundance and no change in renin protein abundance in the renal cortex. NKCC2 plays a role as a sensor in the initial response to altered luminal NaCl concentration and thus in the induction of the TGF (32), by a mechanism that involves an adaption of COX-2 expression and PGE_2 synthesis in the macula densa and cortical TALH cells

(10). Absent NKCC2 ion transport in macula densa cells, e.g., by known mutations in humans or furosemide treatment, indicates a false signal of low tubular Cl concentration, leading to increased expression of COX-2, increased synthesis of macula densa PGE_2, and increased renin expression and secretion (10). However, in our mutant mouse line, no hints on activation of the macula densa cells and the renin system are existent. Furthermore, urinary excretion of PGE_2 was increased (however, less than in the human disease), but it cannot be deduced from this result that PGE_2 production was also increased in macula densa cells because they make up an extremely small fraction of all PGE_2-producing cells in the kidney. At the present time, the reason for an absence of activation of renin expression and secretion in the face of apparently decreased NKCC2 activity (consisting of a putatively impaired ion transport capacity and/or highly reduced protein abundance of mutant NKCC2) is not clear in our mutant mouse line. Linkage analysis excludes additional causative mutations outside the determined 10-Mb region (120.3–130.5 Mb) of chromosome 2. Although the probability of the existence of confounding nonsegregating mutations within this chromosomal region is $P < 0.001$, and further bioinformatic and genetic analyses carried out in this study did not show further mutations, we cannot totally exclude a second mutation within this chromosomal region in a noncoding region or a gene with so far unknown impact on renal function, macula densa and RAAS. Therefore, further studies are needed to better evaluate the influence of mutant NKCC2 on macula densa cells, TGF, and COX-2 expression, and to explain the absence of hyperreninemia in homozygous $Slc12a1^{I1299F}$ mutant mice. As a consequence of the unstimulated renin system, aldosterone secretion was also not stimulated in our mutant mice, in contrast to affected humans who exhibit hyperaldosteronism secondary to hyperreninemia.

Clinical symptoms of type I Bartter syndrome in humans often appear before birth, in the last trimenon of pregnancy (28). However, Pressler and colleagues (27) described a case of two siblings with the onset of clinical symptoms during puberty, representing a late-onset manifestation of type I Bartter syndrome as a result of a residual function of the mutant NKCC2 transporter (27). Similar to this human case report, the onset of clinical symptoms in homozygous mutant mice occurred in their early postnatal life. Thus, according to the definition of type I Bartter syndrome with a proven mutation in the *SLC12A1* gene in humans, the $Slc12a1^{I1299F}$ mutant mouse line represents a viable animal model for late-onset manifes-

tation of this human disease, highlighting the broad facets of NKCC2 dysfunction.

In heterozygous mutant mice, only mild deviations were found. NKCC2 usually assembles as a dimer, in which the individual subunits transport Na^+ independently (40). In addition, there might be a considerable reserve capacity of NKCC2 ion transport as only 2–3% of total NKCC2 protein is located at the cell surface of TALH under basal conditions (24). This might explain the recessive mode of inheritance of mutations of *SLC12A1* in humans as well as in the mutant mouse line.

In conclusion, we have established a novel mutant mouse line, *Slc12a1*[I299F], harboring a novel allelic NKCC2 variant. These mice exhibit a phenotype that shares many but not all of the symptoms described in humans suffering from type I Bartter syndrome. The polyuria observed in this model, and possibly also that in the human disease, may be due to the combination of two different additive factors, a decrease in activity of NKCC2, and a urea-selective concentrating defect which probably results from an increased medullary blood flow induced by medullary prostaglandins. These hypotheses need further confirmation. The reasons for the discrepancies between this mouse model and the human disease remain to be elucidated. The unstimulated renin system in this mutant mouse model suggests that heritable polyuria without hyper-reninemia in humans should not exclude *SLC12A1* as a candidate gene for the causative mutation.

DISCLOSURES

No conflicts of interest are declared by the authors.

REFERENCES

1. **Aigner B, Rathkolb B, Herbach N, Kemter E, Schessl C, Klaften M, Klempt M, Hrabé de Angelis M, Wanke R, Wolf E.** Screening for increased plasma urea levels in a large-scale ENU mouse mutagenesis project reveals kidney disease models. *Am J Physiol Renal Physiol* 292: F1560–F1567, 2007.
2. **Bates JM, Raffi HM, Prasadan K, Mascarenhas R, Laszik Z, Maeda N, Hultgren SJ, Kumar S.** Tamm-Horsfall protein knockout mice are more prone to urinary tract infection: rapid communication. *Kidney Int* 65: 791–797, 2004.
3. **Bhagat CI, Garcia-Webb P, Fletcher E, Beilby JP.** Calculated vs measured plasma osmolalities revisited. *Clin Chem* 30: 1703–1705, 1984.
4. **Choi HK, Mount DB, Reginato AM.** Pathogenesis of gout. *Ann Intern Med* 143: 499–516, 2005.
5. **Chuang EL, Reineck HJ, Osgood RW, Kunau RT Jr, Stein JH.** Studies on the mechanism of reduced urinary osmolality after exposure of renal papilla. *J Clin Invest* 61: 633–639, 1978.
6. **Colussi G, Rombola G, Airaghi C, De Ferrari ME, Minetti L.** Pseudo-Bartter's syndrome from surreptitious diuretic intake: differential diagnosis with true Bartter's syndrome. *Nephrol Dial Transplant* 7: 896–901, 1992.
7. **Gailus-Durner V, Fuchs H, Becker L, Bolle I, Brielmeier M, Calzada-Wack J, Elvert R, Ehrhardt N, Dalke C, Franz TJ, Grundner-Culemann E, Hammelbacher S, Holter SM, Holzlwimmer G, Horsch M, Javaheri A, Kalaydjiev SV, Klempt M, Kling E, Kunder S, Lengger C, Lisse T, Mijalski T, Naton B, Pedersen V, Prehn C, Przemeck G, Racz I, Reinhard C, Reitmeir P, Schneider I, Schrewe A, Steinkamp R, Zybill C, Adamski J, Beckers J, Behrendt H, Favor J, Graw J, Heldmaier G, Hofler H, Ivandic B, Katus H, Kirchhof P, Klingenspor M, Klopstock T, Lengeling A, Muller W, Ohl F, Ollert M, Quintanilla-Martinez L, Schmidt J, Schulz H, Wolf E, Wurst W, Zimmer A, Busch DH, Hrabé de Angelis M.** Introducing the German Mouse Clinic: open access platform for standardized phenotyping. *Nat Methods* 2: 403–404, 2005.
8. **Gamba G.** Molecular physiology and pathophysiology of electroneutral cation-chloride cotransporters. *Physiol Rev* 85: 423–493, 2005.
9. **Greger R.** Ion transport mechanisms in thick ascending limb of Henle's loop of mammalian nephron. *Physiol Rev* 65: 760–797, 1985.
10. **Hao CM, Breyer MD.** Physiological regulation of prostaglandins in the kidney. *Annu Rev Physiol* 70: 357–377, 2008.
11. **Hoelter SM, Dalke C, Kallnik M, Becker L, Horsch M, Schrewe A, Favor J, Klopstock T, Beckers J, Ivandic B, Gailus-Durner V, Fuchs H, Hrabé de Angelis M, Graw J, Wurst W.** "Sighted C3H" mice–a tool for analysing the influence of vision on mouse behaviour? *Front Biosci* 13: 5810–5823, 2008.
12. **Hrabé de Angelis M, Flaswinkel H, Fuchs H, Rathkolb B, Soewarto D, Marschall S, Heffner S, Pargent W, Wuensch K, Jung M, Reis A, Richter T, Alessandrini F, Jakob T, Fuchs E, Kolb H, Kremmer E, Schaeble K, Rollinski B, Roscher A, Peters C, Meitinger T, Strom T, Steckler T, Holsboer F, Klopstock T, Gekeler F, Schindewolf C, Jung T, Avraham K, Behrendt H, Ring J, Zimmer A, Schughart K, Pfeffer K, Wolf E, Balling R.** Genome-wide, large-scale production of mutant mice by ENU mutagenesis. *Nat Genet* 25: 444–447, 2000.
13. **Isenring P, Jacoby SC, Chang J, Forbush B.** Mutagenic mapping of the Na-K-Cl cotransporter for domains involved in ion transport and bumetanide binding. *J Gen Physiol* 112: 549–558, 1998.
14. **Justice MJ, Noveroske JK, Weber JS, Zheng B, Bradley A.** Mouse ENU mutagenesis. *Hum Mol Genet* 8: 1955–1963, 1999.
15. **Keays DA, Clark TG, Campbell TG, Broxholme J, Valdar W.** Estimating the number of coding mutations in genotypic and phenotypic driven *N*-ethyl-*N*-nitrosourea (ENU) screens: revisited. *Mamm Genome* 18: 123–124, 2007.
16. **Kemter E, Philipp U, Klose R, Kuiper H, Boelhauve M, Distl O, Wolf E, Leeb T.** Molecular cloning, expression analysis and assignment of the porcine tumor necrosis factor superfamily member 10 gene (TNFSF10) to SSC13q34–>q36 by fluorescence in situ hybridization and radiation hybrid mapping. *Cytogenet Genome Res* 111: 74–78, 2005.
17. **Kemter E, Rathkolb B, Rozman J, Hans W, Schrewe A, Landbrecht C, Klaften M, Ivandic B, Fuchs H, Gailus-Durner V, Klingenspor M, de Angelis MH, Wolf E, Wanke R, Aigner B.** Novel missense mutation of uromodulin in mice causes renal dysfunction with alterations in urea handling, energy, and bone metabolism. *Am J Physiol Renal Physiol* 297: F1391–F1398, 2009.
18. **Kim SM, Chen L, Mizel D, Huang YG, Briggs JP, Schnermann J.** Low plasma renin and reduced renin secretory responses to acute stimuli in conscious COX-2-deficient mice. *Am J Physiol Renal Physiol* 292: F415–F422, 2007.
19. **Klose R, Kemter E, Bedke T, Bittmann I, Kessler B, Endres R, Pfeffer K, Schwinzer R, Wolf E.** Expression of biologically active human TRAIL in transgenic pigs. *Transplantation* 80: 222–230, 2005.
20. **Lee HW, Kim WY, Song HK, Yang CW, Han KH, Kwon HM, Kim J.** Sequential expression of NKCC2, TonEBP, aldose reductase, and urea transporter-A in developing mouse kidney. *Am J Physiol Renal Physiol* 292: F269–F277, 2007.
21. **Mo L, Zhu XH, Huang HY, Shapiro E, Hasty DL, Wu XR.** Ablation of the Tamm-Horsfall protein gene increases susceptibility of mice to bladder colonization by type 1-fimbriated *Escherichia coli*. *Am J Physiol Renal Physiol* 286: F795–F802, 2004.
22. **Oppermann M, Mizel D, Huang G, Li C, Deng C, Theilig F, Bachmann S, Briggs J, Schnermann J, Castrop H.** Macula densa control of renin secretion and preglomerular resistance in mice with selective deletion of the B isoform of the Na,K,2Cl co-transporter. *J Am Soc Nephrol* 17: 2143–2152, 2006.

23. **Oppermann M, Mizel D, Kim SM, Chen L, Faulhaber-Walter R, Huang Y, Li C, Deng C, Briggs J, Schnermann J, Castrop H.** Renal function in mice with targeted disruption of the A isoform of the Na-K-2Cl co-transporter. *J Am Soc Nephrol* 18: 440–448, 2007.

24. **Ortiz PA.** cAMP increases surface expression of NKCC2 in rat thick ascending limbs: role of VAMP. *Am J Physiol Renal Physiol* 290: F608–F616, 2006.

25. **Pak J, Pu Y, Zhang ZT, Hasty DL, Wu XR.** Tamm-Horsfall protein binds to type 1 fimbriated *Escherichia coli* and prevents *E. coli* from binding to uroplakin Ia and Ib receptors. *J Biol Chem* 276: 9924–9930, 2001.

26. **Peters M, Jeck N, Reinalter S, Leonhardt A, Tonshoff B, Klaus GG, Konrad M, Seyberth HW.** Clinical presentation of genetically defined patients with hypokalemic salt-losing tubulopathies. *Am J Med* 112: 183–190, 2002.

27. **Pressler CA, Heinzinger J, Jeck N, Waldegger P, Pechmann U, Reinalter S, Konrad M, Beetz R, Seyberth HW, Waldegger S.** Late-onset manifestation of antenatal Bartter syndrome as a result of residual function of the mutated renal Na$^+$-K$^+$-2Cl$^-$ Co-transporter. *J Am Soc Nephrol* 17: 2136–2142, 2006.

28. **Proesmans W.** Bartter syndrome and its neonatal variant. *Eur J Pediatr* 156: 669–679, 1997.

29. **Reinalter SC, Jeck N, Peters M, Seyberth HW.** Pharmacotyping of hypokalaemic salt-losing tubular disorders. *Acta Physiol Scand* 181: 513–521, 2004.

30. **Rodriguez-Soriano J, Vallo A, Aguirre M.** Bone mineral density and bone turnover in patients with Bartter syndrome. *Pediatr Nephrol* 20: 1120–1125, 2005.

31. **Scherer B, Schnermann J, Sofroniev M, Weber PC.** Prostaglandin (PG) analysis in urine of humans and rats by different radioimmunoassays: effect on PG-excretion by PG-synthetase inhibitors, laparotomy and furosemide. *Prostaglandins* 15: 255–266, 1978.

32. **Schnermann J, Briggs JP.** Tubuloglomerular feedback: mechanistic insights from gene-manipulated mice. *Kidney Int* 74: 418–426, 2008.

33. **Schoensiegel F, Bekeredjian R, Schrewe A, Weichenhan D, Frey N, Katus HA, Ivandic BT.** Atrial natriuretic peptide and osteopontin are useful markers of cardiac disorders in mice. *Comp Med* 57: 546–553, 2007.

34. **Schroter J, Timmermans G, Seyberth HW, Greven J, Bachmann S.** Marked reduction of Tamm-Horsfall protein synthesis in hyperprostaglandin E-syndrome. *Kidney Int* 44: 401–410, 1993.

35. **Scolari F, Caridi G, Rampoldi L, Tardanico R, Izzi C, Pirulli D, Amoroso A, Casari G, Ghiggeri GM.** Uromodulin storage diseases: clinical aspects and mechanisms. *Am J Kidney Dis* 44: 987–999, 2004.

36. **Seyberth HW, Rascher W, Schweer H, Kuhl PG, Mehls O, Scharer K.** Congenital hypokalemia with hypercalciuria in preterm infants: a hyperprostaglandinuric tubular syndrome different from Bartter syndrome. *J Pediatr* 107: 694–701, 1985.

37. **Shoemaker L, Welch TR, Bergstrom W, Abrams SA, Yergey AL, Vieira N.** Calcium kinetics in the hyperprostaglandin E syndrome. *Pediatr Res* 33: 92–96, 1993.

38. **Sica D, Schollwerth A.** Renal handling of organic anions and cations and renal excretion of uric acid. In: *The Kidney*, edited by Brenner BM. Philadelphia, PA: Saunders, 1996, p. 607–700.

39. **Simon DB, Karet FE, Hamdan JM, DiPietro A, Sanjad SA, Lifton RP.** Bartter's syndrome, hypokalaemic alkalosis with hypercalciuria, is caused by mutations in the Na-K-2Cl cotransporter NKCC2. *Nat Genet* 13: 183–188, 1996.

40. **Starremans PG, Kersten FF, Knoers NV, Van Den Heuvel LP, Bindels RJ.** Mutations in the human Na-K-2Cl cotransporter (NKCC2) identified in Bartter syndrome type I consistently result in nonfunctional transporters. *J Am Soc Nephrol* 14: 1419–1426, 2003.

41. **Stokes JB.** Integrated actions of renal medullary prostaglandins in the control of water excretion. *Am J Physiol Renal Fluid Electrolyte Physiol* 240: F471–F480, 1981.

42. **Tajiri J, Nakayama M, Sato T, Isozaki S, Uchino K.** Pseudo-Bartter's syndrome due to furosemide abuse: report of a case and an analytical review of Japanese literature. *Jpn J Med* 20: 216–221, 1981.

43. **Takahashi N, Chernavvsky DR, Gomez RA, Igarashi P, Gitelman HJ, Smithies O.** Uncompensated polyuria in a mouse model of Bartter's syndrome. *Proc Natl Acad Sci USA* 97: 5434–5439, 2000.

44. **Tovar-Palacio C, Bobadilla NA, Cortes P, Plata C, de los Heros P, Vazquez N, Gamba G.** Ion and diuretic specificity of chimeric proteins between apical Na$^+$-K$^+$-2Cl$^-$ and Na$^+$-Cl$^-$ cotransporters. *Am J Physiol Renal Physiol* 287: F570–F577, 2004.

45. **Yang B, Bankir L.** Urea and urine concentrating ability: new insights from studies in mice. *Am J Physiol Renal Physiol* 288: F881–F896, 2005.